Synthesis, *X*-Ray Characterization, and *Q*-Band Electron Spin Resonance Studies of Heterometallic, Polymeric Compounds formed by Yttrium and Lanthanide(III) Nitrates with HgL_2 (L = C_4H_6NO, the Anion of 2-Pyrrolidone); Crystal Structures of $[\{Hg_2EuL_4(NO_3)_3\}_n]$ and $[\{Hg_3Tb_2L_6(NO_3)_6\}_n]$ †

David M. L. Goodgame,* David J. Williams, and Richard E. P. Winpenny
Chemistry Department, Imperial College of Science and Technology, London SW7 2AY

The complex HgL_2 (L = C_4H_6NO, the anion of 2-pyrrolidone) reacts with lanthanide(III) nitrates, Ln = La to Gd (Pm not studied), in methanol to give $[\{Hg_2LnL_4(NO_3)_3\}_n]$, and with Y and Ln = Tb to Yb to yield $[\{Hg_3Y_2L_6(NO_3)_6\}_n]$ and $[\{Hg_3Ln_2L_6(NO_3)_6\}_n]$ respectively. Each set of compounds forms an isostructural series, representative members of which, Ln = Eu and Tb respectively, have been characterized by single-crystal *X*-ray diffraction methods. Both compounds form polymeric chains involving 16-membered macrocycles. They differ in that the europium complex comprises continuous chains of rings interlocked at the lanthanide ion, whereas in the terbium compound each macrocycle is separated from its neighbour by an additional HgL_2 unit. In both instances the lanthanide ion is nine-co-ordinate and the polymeric chains are cross-linked by nitrate anions. *Q*-Band e.s.r. spectra were obtained for gadolinium(III)-doped powder samples of seven of the complexes and also for $[\{Hg_2ThL_4(NO_3)_4\}_n]$ and the zero-field splitting parameters, D and λ, were obtained from the allowed transitions. Additional, much weaker sets of bands in the low-field (0—725 mT) region arising from various off-axis, in-plane and off-axis, out-of-plane turning points of forbidden ($\Delta M_S \neq \pm 1$) transitions are reported and assigned.

Recently we have reported initial results of our investigations into the ability of the anion of 2-pyrrolidone (=L) to link dissimilar metal ions to produce unusual new polynuclear compounds.[1] We have shown that there is sufficient differentiation between the metal binding preferences of the deprotonated ring nitrogen and the exocyclic oxygen to permit a heavy post-transition metal, such as mercury, to bind to the nitrogen alone, while leaving the oxygen free to co-ordinate to a wide range of other metal ions [*e.g.* copper(II),[1a] cobalt(II),[1b] and silver(I)[1d]].

For both copper(II) and cobalt(II) unusual extended structures resulted, a layer polymer consisting of contiguous 32-membered macrocycles in the case of $[\{Hg_2Cu(C_4H_6NO)_4X_2\}_n]$ (X = NO_3 or ClO_4),[1a] but a chain polymer comprising 16-membered macrobicyclic links in $\{[Hg_3Co(C_4H_6NO)_6][NO_3]_2\}_n$.[1b] In view of these results and the current interest in new heterometallic solid-state materials involving yttrium and the lanthanide ions, we have explored the preparation and properties of related compounds formed by $Hg(C_4H_6NO)_2$ with yttrium(III) and the *f*-block metal ions. We report here the results of our synthetic, structural, and spectroscopic studies on these complexes. A brief account of some of the results has been given in a preliminary communication.[1c]

Experimental

Preparation of Compounds.—The compound $Hg(C_4H_6NO)_2$ (**1**) was prepared as described previously.[1b] The heterometallic complexes (see Table 1) were prepared by reacting (**1**) (1 mmol) with the appropriate hydrated metal nitrate (0.2—0.25 mmol) in methanol (20 cm^3). The initial precipitate, which formed in periods varying from 5 min to 1 h depending on the metal used, was removed by filtration and the filtrate allowed to evaporate at room temperature. For compounds (**7**) and (**9**) small colourless crystals suitable for *X*-ray analysis formed after 3 d. Compounds (**2**)—(**6**), (**8**), and (**10**)—(**15**) gave microcrystalline products in the same period.

Analytical data (Microanalytical Laboratory, Imperial College) and other physical data are given in Table 1.

The gadolinium(III)-doped compounds were prepared by an identical procedure, with the addition of *ca.* 1 mol% $Gd(NO_3)_3 \cdot 5H_2O$ to the reaction solution.

Spectroscopy.—I.r. spectra were recorded on a Perkin-Elmer 1720 FT spectrometer as Nujol mulls (CsI), u.v.-visible reflectance spectra on a Beckman DK2 spectrometer on powder samples. E.s.r. spectra were measured at room temperature on polycrystalline samples using a *Q*-band spectrometer comprising a Varian 36-GHz microwave bridge and a Newport 12-in type F magnet powered by a C905 rotary generator and post stabilizer. Spin-Hamiltonian parameters were calculated using the method outlined by Reynolds *et al.*[2] and these values were checked by calculating resonance fields using the program[3] ESRS. *X*-Ray powder diffraction experiments were carried out on a Guinier focusing camera using Cu-K_α radiation.

Crystallography.—Crystal data. $[\{Hg_2Eu(C_4H_6NO)_4(NO_3)_3\}_n]$ (**7**), $C_{16}H_{24}EuHg_2N_7O_{13}$, M = 1075.5, monoclinic, a = 9.879(2), b = 14.594(3), c = 18.211(3) Å, β = 93.58(2)°, U = 2 631 Å^3, space group $P2_1/c$, Z = 4, D_c = 2.72 g cm^{-3}, μ(Cu-K_α) = 391 cm^{-1}, λ = 1.541 78 Å, $F(000)$ = 1 971. Colourless, air-stable hexagonal plates, crystal dimensions 0.03 × 0.19 × 0.20 mm.

$[\{Hg_3Tb_2(C_4H_6NO)_6(NO_3)_6\}_n]$ (**9**), $C_{24}H_{36}Hg_3N_{12}O_{24}Tb_2$, M = 1 796.2, monoclinic, a = 11.833(4), b = 13.070(2), c = 14.435(3) Å, β = 98.65(2)°, U = 2 207 Å^3, space group $P2_1/c$, Z = 2, D_c = 2.71 g cm^{-3}, μ(Cu-K_α) = 360 cm^{-1}, λ = 1.541 78 Å, $F(000)$ = 1 640. Colourless, air-stable square plates, crystal dimensions 0.01 × 0.18 × 0.20 mm.

Data collection and processing. Nicolet R3m diffractometer,

† *Supplementary data available:* see Instructions for Authors, *J. Chem. Soc., Dalton Trans.*, 1989, Issue 1, pp. xvii—xx.

Table 1. Analytical[a] and physical data for the compounds

	Complex	Colour	M.p.[b] (°C)	ν(CO)/cm^{-1}	Analysis (%) C	H	N
(2)	$[Hg_2La(C_4H_6NO)_4(NO_3)_3]$	White	158—161	1 582	18.2 (18.1)	2.1 (2.3)	9.0 (9.2)
(3)	$[Hg_2Ce(C_4H_6NO)_4(NO_3)_3]$	White	*c*	1 581	18.1 (18.1)	2.2 (2.3)	9.0 (9.2)
(4)	$[Hg_2Pr(C_4H_6NO)_4(NO_3)_3]$	Green	157—159	1 582	17.8 (18.1)	2.1 (2.3)	9.0 (9.2)
(5)	$[Hg_2Nd(C_4H_6NO)_4(NO_3)_3]$	Lilac	*c*	1 581	17.7 (18.0)	2.1 (2.3)	9.1 (9.2)
(6)	$[Hg_2Sm(C_4H_6NO)_4(NO_3)_3]$	Cream	157—159	1 582	17.9 (17.9)	2.2 (2.3)	9.0 (9.1)
(7)	$[Hg_2Eu(C_4H_6NO)_4(NO_3)_3]$	White	160—163	1 582	17.8 (17.9)	2.1 (2.3)	9.0 (9.1)
(8)	$[Hg_2Gd(C_4H_6NO)_4(NO_3)_3]$	White	181—185	1 592	18.0 (17.8)	2.1 (2.2)	8.9 (9.1)
(9)	$[Hg_3Tb_2(C_4H_6NO)_6(NO_3)_6]$	White	159—162	1 575	16.0 (16.1)	1.9 (2.0)	9.1 (9.4)
(10)	$[Hg_3Dy_2(C_4H_6NO)_6(NO_3)_6]$	Cream	159—162	1 575	16.2 (16.0)	2.0 (2.0)	9.1 (9.3)
(11)	$[Hg_3Ho_2(C_4H_6NO)_6(NO_3)_6]$	Cream	160—163	1 575	16.0 (15.9)	1.9 (2.0)	9.1 (9.3)
(12)	$[Hg_3Er_2(C_4H_6NO)_6(NO_3)_6]$	Lilac	158—161	1 575	16.5 (15.9)	2.0 (2.0)	9.3 (9.3)
(13)	$[Hg_3Tm_2(C_4H_6NO)_6(NO_3)_6]$	Very pale green	159—162	1 576	16.0 (15.9)	2.0 (2.0)	9.2 (9.3)
(14)	$[Hg_3Yb_2(C_4H_6NO)_6(NO_3)_6]$	White	150—153	1 576	15.8 (15.8)	1.9 (2.0)	9.0 (9.2)
(15)	$[Hg_3Y_2(C_4H_6NO)_6(NO_3)_6]$	White	156—159	1 576	17.3 (17.4)	2.1 (2.2)	9.9 (10.2)

[a] Required values are given in parentheses. [b] With decomposition. [c] No clear decomposition point.

ω-scan method ($2\theta \leqslant 116°$), graphite-monochromated Cu-K_α radiation. For compounds (**7**) and (**9**) 3 663 and 3 208 independent reflections were measured; 2 707 and 2 282, respectively, considered observed [$|F_o| > 3\sigma(|F_o|)$], corrected for Lorentz and polarization factors. For (**7**) a Gaussian absorption correction (face-indexed crystal) was applied, minimum and maximum transmission factors 0.02 and 0.33; for (**9**) an empirical absorption correction [lamina, (100) prominent] based on 279 azimuthal measurements was applied, minimum and maximum transmission factors 0.14 and 0.70.

Structure analysis and refinement. The structures were solved by the heavy-atom method which in both cases revealed the position of one of the mercury atoms. All remaining non-hydrogen atoms were located from subsequent ΔF maps and refined anisotropically. The hydrogen atoms were idealized (C–H 0.96 Å), assigned isotropic thermal parameters, $U(H) = 1.2_{eq}(C)$, and allowed to ride on their parent carbons. Refinement was by block-cascade full-matrix least squares to give: for (**7**), $R = 0.046$, $R' = 0.044$ [$w^{-1} = \sigma^2(F) + 0.000\,60F^2$]; for (**9**), $R = 0.036$, $R' = 0.035$ [$w^{-1} = \sigma^2(F) + 0.000\,22F^2$] ($R = \sum[|F_o| - |F_c|]/\sum|F_o|$). The maximum residual electron densities in the final ΔF maps were 1.3 and 0.9 e Å^{-3} for (**7**) and (**9**) respectively. The mean and maximum shift/error ratios in the final refinement cycle were: for (**7**), 0.00 and 0.06; for (**9**) 0.02 and 0.06. Computations were carried out on an Eclipse S140 computer using the SHELXTL program system[4] and published scattering factors.[5] Atomic co-ordinates are listed in Tables 2 and 3, and important bond lengths and angles in Tables 4 and 5.

Additional material available from the Cambridge Crystallographic Data Centre comprises H-atom co-ordinates, thermal parameters, and remaining bond lengths and angles.

Results and Discussion

The stoicheiometries of the solid products obtained from the reaction of methanolic solutions of $Hg(C_4H_6NO)_2$ and yttrium or lanthanide(III) nitrates depend on the lanthanide ion employed. Use of the trivalent lanthanide ions in the series La to Gd (Pm not studied) afforded the compounds $[Hg_2Ln(C_4H_6NO)_4(NO_3)_3]$, whereas yttrium and the lanthanides in the series terbium to ytterbium inclusive gave compounds of stoicheiometry $[Hg_3Ln_2(C_4H_6NO)_6(NO_3)_6]$. Alterations in the mole ratios of Hg:Ln did not result in any change in the composition of members of each respective series of complexes. Instead, the size of the lanthanide (or yttrium) ion appears to influence which complex type is formed, with the change occurring on passing from Gd^{3+} to Tb^{3+}, and with Y^{3+} adopting the same type as the smaller lanthanide ions.

Structures.—*X*-Ray powder diffraction measurements showed that all the compounds within each respective series are isostructural. The data, which were obtained photographically, were adequate to establish the isomorphous character of the related compounds, but not sufficiently resolved to permit accurate indexing and accurate lattice parameter determination. A representative member of each series, $[Hg_2Eu(C_4H_6NO)_4(NO_3)_3]$ (**7**) and $[Hg_3Tb_2(C_4H_6NO)_6(NO_3)_6]$ (**9**) were obtained in a form suitable for single-crystal *X*-ray analysis.

Co-ordination geometries. In both cases the lanthanides (Eu and Tb) are bound to nine O atoms (Figures 1 and 2). In (**7**) four of these O atoms come from the 2-pyrrolidone ligands and five from nitrate groups, whilst in (**9**) the division is three and six respectively.

In both compounds the M–O bond lengths depend markedly on the origin of the oxygen donor atoms. The shortest M–O bonds involve oxygen atoms from the 2-pyrrolidone ligands [*ca.*

Table 2. Atom co-ordinates ($\times 10^4$) with estimated standard deviations in parentheses for $[\{Hg_2Eu(C_4H_6NO)_4(NO_3)_3\}_n]$ (**7**)

Atom	*x*	*y*	*z*
Hg(1)	−600(1)	589(1)	3 747(1)
Hg(2)	−609(1)	−468(1)	1 456(1)
Eu	194(1)	2 426(1)	1 902(1)
O(1)	−1 332(10)	3 392(8)	2 446(6)
O(2)	728(9)	2 394(8)	3 179(5)
O(3)	−1 543(8)	1 365(7)	2 160(6)
O(4)	1 544(10)	3 745(7)	2 068(6)
O(51)	1 144(10)	801(8)	2 330(6)
O(52)	2 619(11)	1 762(8)	2 048(7)
O(53)	3 252(12)	370(9)	2 367(8)
O(61)	358(11)	1 220(9)	880(6)
O(62)	1 486(12)	2 437(9)	705(6)
O(63)	1 606(14)	1 267(11)	−35(7)
O(71)	−1 645(13)	2 634(10)	850(7)
O(72)	−464(14)	3 821(10)	882(10)
O(73)	−1 978(14)	3 627(11)	−2(7)
N(1)	−1 211(11)	3 897(9)	3 613(7)
N(2)	1 210(11)	1 242(9)	4 016(6)
N(3)	−2 430(10)	203(8)	1 444(7)
N(4)	2 420(11)	4 949(8)	1 450(6)
N(5)	2 340(12)	969(10)	2 260(7)
N(6)	1 157(11)	1 626(10)	495(7)
N(7)	−1 378(13)	3 388(11)	574(9)
C(11)	−1 805(13)	3 470(11)	3 049(8)
C(12)	−3 091(16)	3 063(14)	3 268(9)
C(13)	−3 210(15)	3 332(15)	4 069(9)
C(14)	−1 961(22)	3 890(17)	4 289(11)
C(21)	1 498(14)	1 985(11)	3 632(8)
C(22)	2 954(16)	2 262(14)	3 854(9)
C(23)	3 405(15)	1 619(15)	4 461(11)
C(24)	2 303(15)	923(13)	4 500(9)
C(31)	−2 524(14)	997(11)	1 765(8)
C(32)	−3 892(14)	1 426(13)	1 629(10)
C(33)	−4 486(17)	834(15)	1 026(11)
C(34)	−3 681(15)	−22(13)	1 042(10)
C(41)	2 490(15)	4 163(11)	1 791(8)
C(42)	3 936(14)	3 805(13)	1 814(11)
C(43)	4 674(14)	4 436(14)	1 359(10)
C(44)	3 727(15)	5 278(12)	1 224(9)

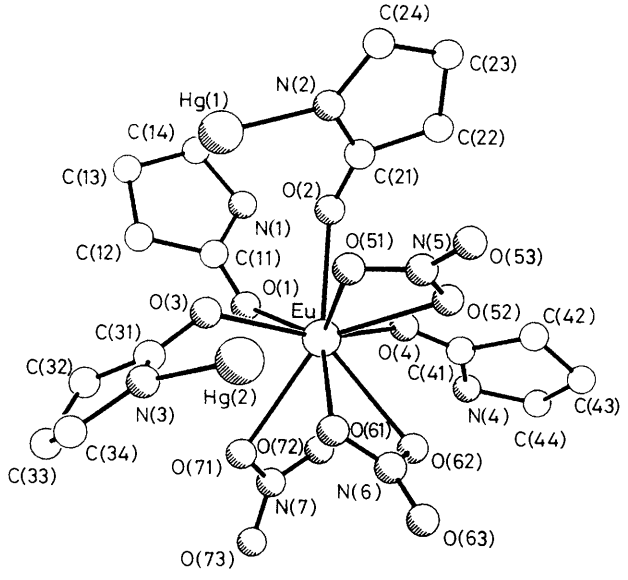

Figure 1. The structure of complex (**7**) in the crystal showing the crystallographic numbering scheme

Table 3. Atom co-ordinates ($\times 10^4$) with estimated standard deviations in parentheses for $[\{Hg_3Tb_2(C_4H_6NO)_6(NO_3)_6\}_n]$ (**9**)

Atom	*x*	*y*	*z*
Hg(1)	110(1)	5 952(1)	8 464(1)
Hg(2)	0	10 000	10 000
Tb	−1 714(1)	6 941(1)	10 799(1)
O(1)	−2 236(6)	5 272(5)	10 555(5)
O(2)	−1 985(6)	6 895(6)	9 209(5)
O(3)	−1 998(6)	8 665(5)	10 579(6)
N(1)	−1 816(7)	3 767(6)	11 292(6)
N(2)	−1 585(7)	5 675(6)	8 190(6)
N(3)	−1 707(7)	9 924(6)	9 585(6)
C(11)	−2 508(9)	4 425(8)	10 841(8)
C(12)	−3 707(10)	4 010(10)	10 696(10)
C(13)	−3 634(11)	3 042(10)	11 242(13)
C(14)	−2 381(10)	2 803(8)	11 515(11)
C(21)	−2 309(9)	6 189(8)	8 607(8)
C(22)	−3 477(10)	5 848(10)	8 326(9)
C(23)	−3 399(11)	5 054(14)	7 536(13)
C(24)	−2 147(10)	4 900(9)	7 559(9)
C(31)	−2 344(9)	9 261(7)	9 903(8)
C(32)	−3 552(10)	9 293(9)	9 381(10)
C(33)	−3 514(13)	10 114(12)	8 670(12)
C(34)	−2 340(11)	10 519(9)	8 801(9)
N(4)	−3 966(9)	7 123(8)	11 332(8)
O(41)	−3 830(7)	7 045(6)	10 487(5)
O(42)	−3 046(7)	7 121(8)	11 911(7)
O(43)	−4 877(9)	7 233(11)	11 598(9)
N(5)	743(8)	6 991(7)	10 637(7)
O(51)	159(7)	7 798(5)	10 555(6)
O(52)	147(6)	6 165(5)	10 633(6)
O(53)	1 768(7)	6 957(7)	10 740(7)
N(6)	−480(8)	6 618(8)	12 737(7)
O(61)	−515(8)	7 441(6)	12 281(6)
O(62)	−987(8)	5 869(6)	12 325(6)
O(63)	55(8)	6 559(7)	13 531(6)

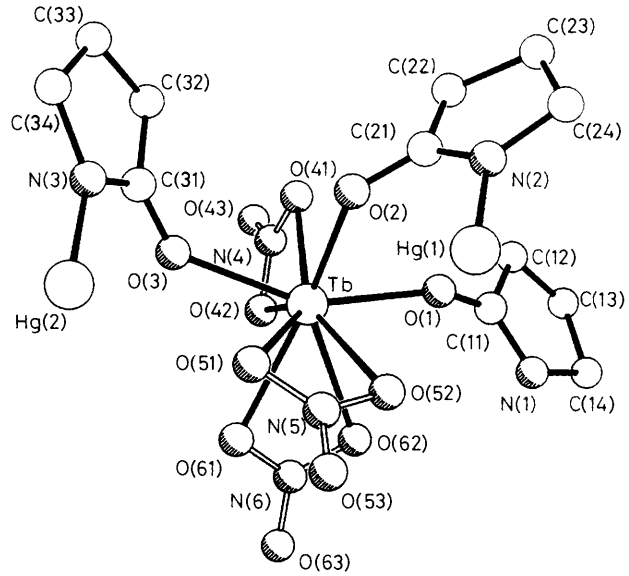

Figure 2. The structure of complex (**9**) in the crystal showing the crystallographic numbering scheme

2.35 Å for (**7**); *ca.* 2.28 Å for (**9**); *cf. ca.* 2.34 Å for (**16**)[6]]. In each compound the M–O (nitrate) distances are longer [*ca.* 2.59 Å for (**7**); *ca.* 2.53 Å for (**9**)]. Similar variations have been reported previously for lanthanide complexes.[7]

The resulting co-ordination geometries can both be regarded as tricapped trigonal prismatic, the upper and lower triangular faces in both compounds being essentially equilateral (angle range 56—64°). They differ, however, in their degrees of

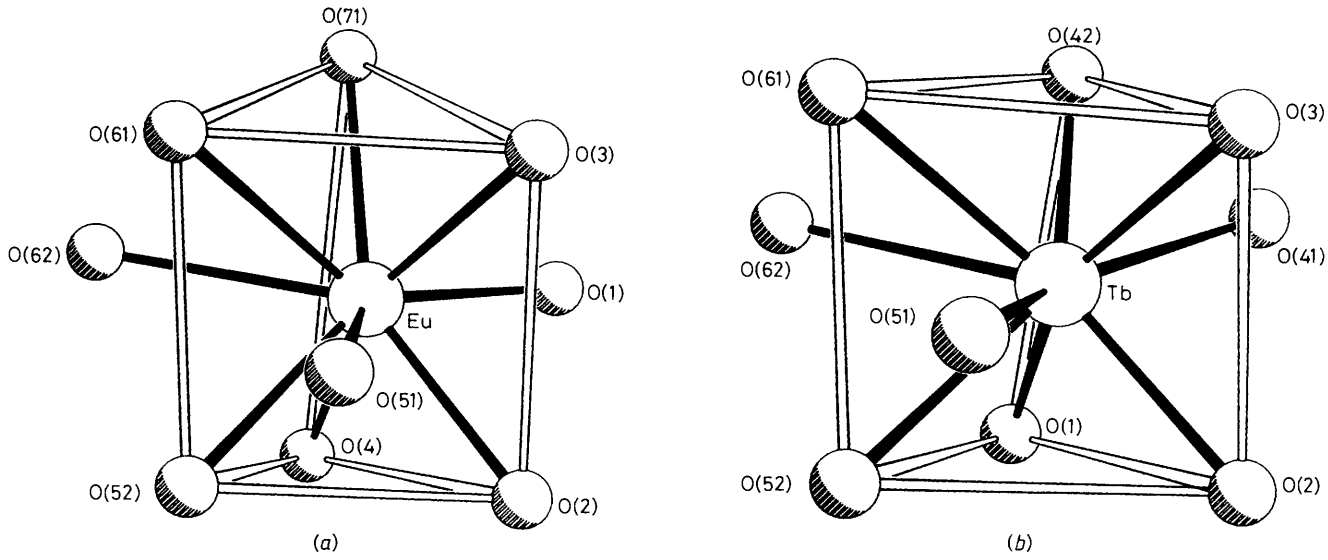

Figure 3. (*a*) Europium co-ordination in complex (**7**). Oxygen–oxygen distances: O(2)···O(3) 3.20, O(2)···O(4) 2.97, O(2)···O(52) 3.01, O(3)···O(61) 3.09, O(3)···O(71) 3.02, O(4)···O(52) 3.08, O(4)···O(71) 4.08, O(52)···O(61) 3.09, and O(61)···O(71) 2.86 Å [average estimated standard deviation (e.s.d.) = 0.01 Å]. (*b*) Terbium co-ordination in complex (**9**). Oxygen–oxygen distances: O(1)···O(2) 2.92, O(1)···O(42) 3.34, O(1)···O(52) 3.04, O(2)···O(3) 3.05, O(2)···O(52) 3.15, O(3)···O(42) 3.17, O(3)···O(61) 3.22, O(42)···O(61) 2.99, and O(52)···O(61) 3.10 Å [average e.s.d = 0.01 Å]

Table 4. Selected bond lengths (Å) and angles (°) for complex (**7**)

Hg(1)–N(2)	2.059(11)	Hg(1)–N(4′)	2.038(11)
Hg(2)–N(3)	2.047(11)	Hg(2)–N(1′)	2.034(11)
Eu–O(1)	2.330(10)	Eu–O(2)	2.353(10)
Eu–O(3)	2.380(10)	Eu–O(4)	2.351(10)
Eu–O(51)	2.650(11)	Eu–O(52)	2.583(11)
Eu–O(61)	2.573(12)	Eu–O(62)	2.593(12)
Eu–O(71)	2.574(13)		
N(2)–Hg(1)–N(4′)	176.4(4)	N(3)–Hg(2)–N(1′)	175.6(5)
O(1)–Eu–O(2)	72.7(3)	O(1)–Eu–O(3)	79.4(4)
O(2)–Eu–O(3)	85.0(3)	O(1)–Eu–O(4)	80.0(4)
O(2)–Eu–O(4)	78.4(4)	O(3)–Eu–O(4)	156.6(4)
O(1)–Eu–O(51)	130.0(4)	O(2)–Eu–O(51)	68.8(4)
O(3)–Eu–O(51)	66.8(3)	O(4)–Eu–O(51)	120.5(3)
O(1)–Eu–O(52)	143.5(4)	O(2)–Eu–O(52)	75.0(4)
O(3)–Eu–O(52)	114.3(3)	O(4)–Eu–O(52)	77.2(3)
O(51)–Eu–O(52)	47.5(3)	O(1)–Eu–O(61)	142.5(3)
O(2)–Eu–O(61)	132.9(4)	O(3)–Eu–O(61)	77.1(4)
O(4)–Eu–O(61)	126.3(4)	O(51)–Eu–O(61)	64.1(4)
O(52)–Eu–O(61)	73.6(4)	O(1)–Eu–O(62)	136.0(4)
O(2)–Eu–O(62)	137.6(3)	O(3)–Eu–O(62)	124.7(4)
O(4)–Eu–O(62)	78.4(4)	O(51)–Eu–O(62)	93.9(4)
O(52)–Eu–O(62)	65.6(4)	O(61)–Eu–O(62)	48.7(4)
O(1)–Eu–O(71)	78.5(4)	O(2)–Eu–O(71)	147.4(4)
O(3)–Eu–O(71)	74.9(4)	O(4)–Eu–O(71)	111.6(4)
O(51)–Eu–O(71)	123.0(4)	O(52)–Eu–O(71)	136.7(4)
O(61)–Eu–O(71)	67.4(4)	O(62)–Eu–O(71)	74.7(4)

Table 5. Selected bond lengths (Å) and angles (°) for complex (**9**)

Hg(1)–N(2)	2.017(8)	Hg(1)–N(1′)	2.029(8)
Hg(2)–N(3)	2.021(8)	Hg(2)–N(3′)	2.021(8)
Tb–O(1)	2.280(7)	Tb–O(2)	2.270(8)
Tb–O(3)	2.293(7)	Tb–O(41)	2.480(8)
Tb–O(42)	2.425(10)	Tb–O(51)	2.555(8)
Tb–O(52)	2.468(8)	Tb–O(61)	2.470(8)
Tb–O(62)	2.644(9)		
N(2)–Hg(1)–N(1′)	178.6(3)	N(3)–Hg(2)–N(3′)	180.0
O(1)–Tb–O(2)	79.9(3)	O(1)–Tb–O(3)	152.6(3)
O(2)–Tb–O(3)	83.7(3)	O(1)–Tb–O(41)	77.4(3)
O(2)–Tb–O(41)	80.4(3)	O(3)–Tb–O(41)	78.3(3)
O(1)–Tb–O(42)	90.4(3)	O(2)–Tb–O(42)	131.7(3)
O(3)–Tb–O(42)	84.3(3)	O(41)–Tb–O(42)	51.4(3)
O(1)–Tb–O(51)	128.2(3)	O(2)–Tb–O(51)	82.3(3)
O(3)–Tb–O(51)	70.3(3)	O(41)–Tb–O(51)	145.5(3)
O(42)–Tb–O(51)	135.5(3)	O(1)–Tb–O(52)	79.4(3)
O(2)–Tb–O(52)	83.3(3)	O(3)–Tb–O(52)	120.3(3)
O(41)–Tb–O(52)	153.6(3)	O(42)–Tb–O(52)	141.5(3)
O(51)–Tb–O(52)	50.3(3)	O(1)–Tb–O(61)	119.6(3)
O(2)–Tb–O(61)	149.1(3)	O(3)–Tb–O(61)	85.0(3)
O(41)–Tb–O(61)	125.1(3)	O(42)–Tb–O(61)	75.4(3)
O(51)–Tb–O(61)	66.8(3)	O(52)–Tb–O(61)	77.8(3)
O(1)–Tb–O(62)	70.6(3)	O(2)–Tb–O(62)	143.8(3)
O(3)–Tb–O(62)	131.2(3)	O(41)–Tb–O(62)	111.9(3)
O(42)–Tb–O(62)	70.3(3)	O(51)–Tb–O(62)	99.6(3)
O(52)–Tb–O(62)	71.3(3)	O(61)–Tb–O(62)	49.2(3)

distortion. In (**7**) the angle between the mean planes of the upper and lower triangular faces [see Figure 3(*a*)] is 22°, whereas in (**9**) the distortion is less, 7° [Figure 3(*b*)]. In both cases the upper and lower faces are out of register; in (**7**) the relative rotation is *ca.* 12° and in (**9**) it is *ca.* 17°. In both compounds the angles between the mean planes of the square faces are within the range 58—63°.

The deviations from planarity of the equatorial LnO_3 planes are small (0.02 Å for Eu and 0.17 Å for Tb), these planes being inclined by 11 and 12° to the upper and lower triangular faces in (**7**) and 3 and 9° in (**9**). The inclinations of the Eu–O(1), Eu–O(51), and Eu–O(62) vectors to the normals of their respective square faces are 2, 12, and 18°; the corresponding values for Tb–O(41), Tb–O(51), and Tb–O(62) are 16, 14, and 12° respectively. The principal cause of these distortions of the geometries is in both cases the small 'bite' of the bidentate NO_3^- anions, and is sufficient to reduce the site symmetry to C_1.

In the related thorium compound $[Hg_2Th(C_4H_6NO)_4(NO_3)_4]$ (**16**)[6] the Th atom is ten-co-ordinate with distorted bicapped antiprismatic geometry, also with C_1 site symmetry.

The polymeric structures. In compounds (**7**) and (**9**) the Hg atoms are bonded to two 2-pyrrolidone ring N atoms and the

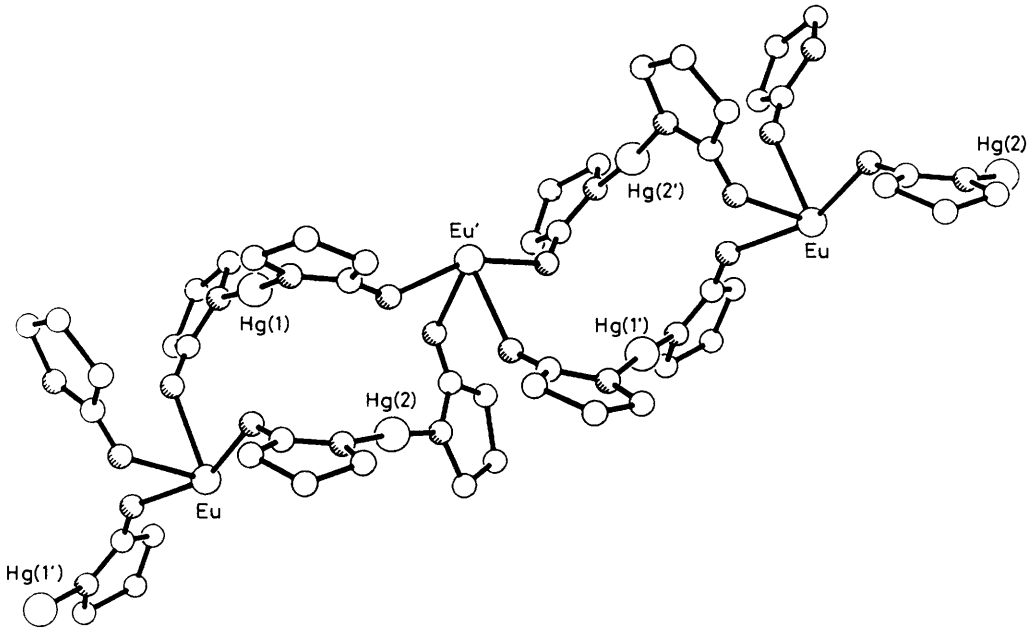

Figure 4. Part of the polymeric chain structure of complex (**7**) showing the interlocking 16-membered rings. The NO_3 groups have been omitted for clarity

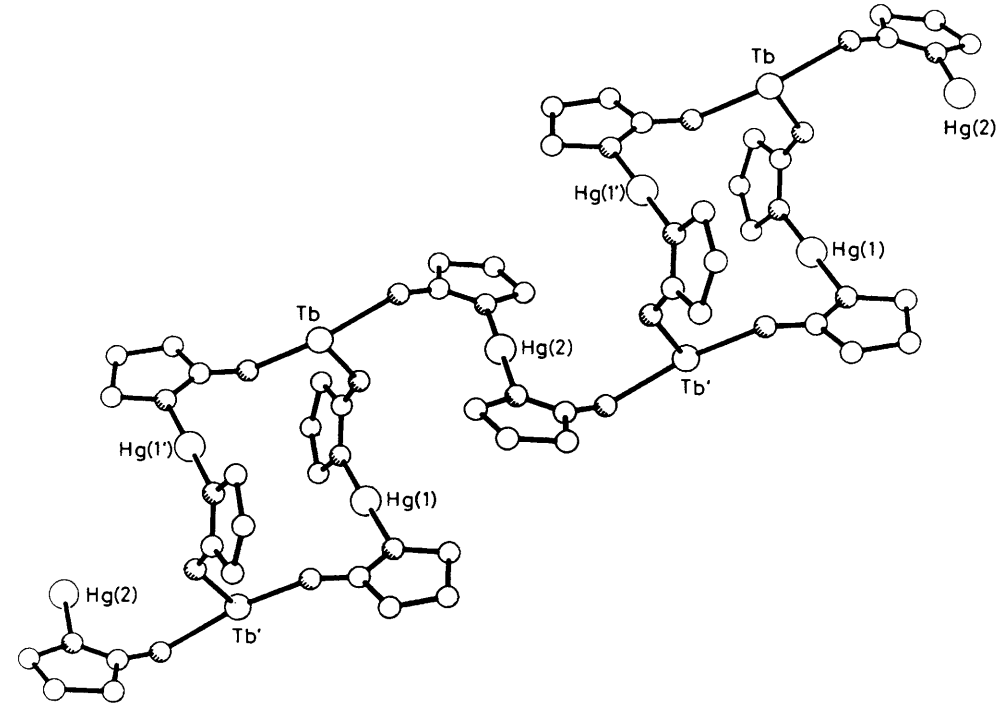

Figure 5. Part of the polymeric chain structure of complex (**9**) showing the alternating 16-membered rings and HgL_2 links. The NO_3 groups have been omitted for clarity

resulting, essentially linear L–Hg–L units bridge adjacent Ln centres forming polymeric chains (Figures 4 and 5). These chains differ appreciably. Although in both instances they contain 16-membered macrocycles, these are linked differently. In (**7**) the macrocycles interlock at the Eu atoms in similar fashion to that observed[6] for (**16**). In (**9**), however, there is an additional HgL_2 unit which links the macrocycles and leads to a different linear polymer type (Figure 5). This marked change may be due to the subtle change in lanthanide co-ordination found in moving from Eu^{III} (**7**) to Tb^{III} (**9**). The smaller ionic radius of Tb^{III} leads to fewer sterically demanding 2-pyrrolidone units being co-ordinated to the rare-earth-metal centre, three rather than four, with the overall co-ordination number remaining at nine as the vacated site is occupied by a less bulky nitrate anion becoming bidentate. This permits the number of ligands bonded to be reduced from seven to six.

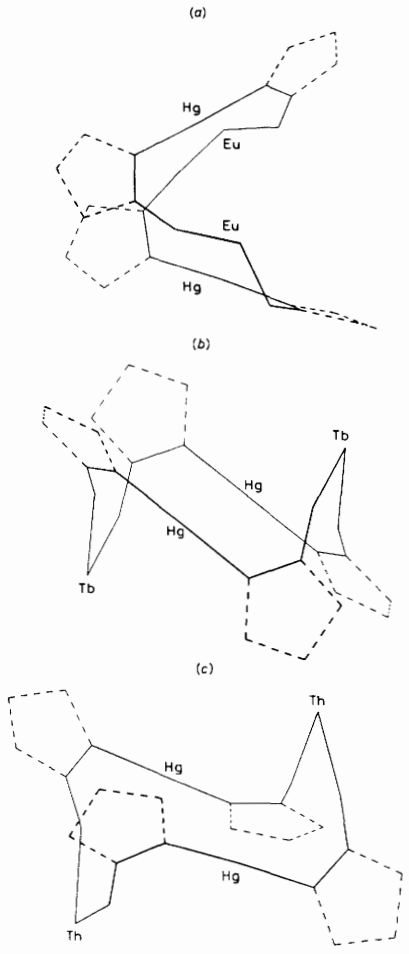

Figure 6. The conformations of the 16-membered macrocycles: (*a*) in complex (**7**); (*b*) in (**9**); and (*c*) in (**16**)

That such a small change in the co-ordination environment leads to such a large change in polymeric structure is a reflection of the conformational flexibility of the HgL_2 unit. This is evidenced by the appreciable variation in the angles between the planes of the 2-pyrrolidone rings bonded to the mercury atoms. Whereas in both compounds (**7**) and (**9**) within each macrocycle the dihedral angle between the pyrrolidone rings is essentially the same (69—74°), in (**9**), in the linking L–Hg–L struts, the two pyrrolidones are coplanar. In the thorium analogue (**16**) the dihedral angles within the macrocyles are 48 and 79°.

Although in both compounds 16-membered macrocycles are formed, their conformations differ appreciably (Figure 6). In (**7**) a 'boat' conformer is formed [Figure 6(*a*)] with the two N–Hg–N units skewed by 55°. The transannular Eu···Eu and Hg···Hg distances are 7.63 and 4.45 Å respectively. In (**9**) a 'chair' conformer is formed [Figure 6(*b*)] with the terbium atoms at the apices, and the N–Hg–N units parallel. The Tb···Tb distance is considerably shorter (7.10 Å) than the equivalent distance in (**7**), and the Hg···Hg distance has increased to 5.13 Å.

In the Th compound (**16**) a 'chair' conformer is also present [Figure 6(*c*)] though the N–Hg–N units are slightly skewed (6°). The Th···Th distance (7.63 Å) is the same as the Eu···Eu distance in (**7**), whilst the Hg···Hg distance (5.21 Å) is similar to that in (**9**).

In both compounds there are inter-chain stabilizing links between nitrate anions in one polymer chain and mercury atoms in the next (Figure 7). These cross-links lie only within

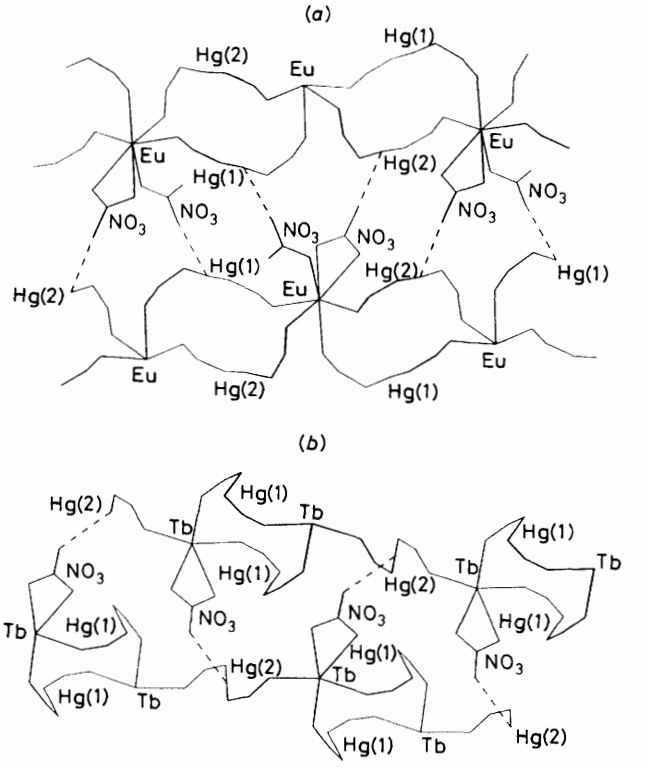

Figure 7. Inter-chain linking by Hg···O (nitrate) interactions: (*a*) in (**7**) and (*b*) in (**9**). For clarity only atoms comprising the macrocycles and relevant nitrates are shown

the crystallographic *bc* plane and the relevant distances are: in (**7**), O(63)···Hg(2) 2.95 and O(73)···Hg(1) 2.96 Å; in (**9**), O(63)···Hg(2) 2.93 Å. Interpolymer interactions of this type are also present in the mercury–thorium compound (**16**),[6] though not in the mercury–copper[1a] or mercury–cobalt[1b] polymers.

E.S.R. Spectra of Gadolinium(III)-doped Compounds.—The availability of the virtually complete series of closely related lanthanide(III)–mercury(II) polymeric complexes and also their yttrium(III) and thorium(IV) analogues has provided the opportunity to explore the use of e.s.r. measurements on gadolinium(III)-doped samples as a probe of the differences in the structures. Gadolinium(III) has a $^8S_{\frac{7}{2}}$ ground state and a long spin–lattice relaxation time which allows its e.s.r. to be observable at all temperatures, making it ideal for such studies.[8]

We have measured the spectra of gadolinium(III)-doped into compounds (**2**), (**3**), (**5**)—(**7**), (**9**), (**15**), and (**16**). A typical signal at *Q*-band frequency for a powder sample is shown in Figure 8. It is convenient to consider two regions in discussing the observed spectra. In the 800—1 600 mT region are found the strong, allowed ($\Delta M_s = \pm 1$) transitions, and at low field we observed a much weaker set of bands arising from forbidden transitions. We shall first consider the allowed transitions.

Although, in principle, an *S* state should have no interactions with crystal fields, in practice fine structure due to zero-field splitting is normally seen in gadolinium(III) spectra.[8] This splitting is generally smaller than that produced by the Zeeman interaction and at room temperature all the resulting levels are appreciably populated. The e.s.r. spectrum of Gd^{III} can therefore be described using the general spin Hamiltonian[9] (1)

$$\mathcal{H} = g\mu_B \vec{H} \cdot \vec{S} + \sum_{n,m} b_n^m O_n^m \qquad (1)$$

Table 6. Calculated spin-Hamiltonian parameters[a] for gadolinium(III)-doped compounds (**2**), (**3**), (**5**)—(**7**), (**9**), (**15**), and (**16**)

M	La	Ce	Nd	Sm	Eu	Tb	Y	Th
Compound	(**2**)	(**3**)	(**5**)	(**6**)	(**7**)	(**9**)	(**15**)	(**16**)
b_2^0	395 (5)	390	380	375	410	410	410	550
b_2^2	200 (5)	205	200	195	275	290	305	300
b_4^0	2 (2)	2	2	2	2	2	2	2
b_4^4	−8 (16)	−7	−9	8	17	−18	−16	−25
b_6^0	0.1 (0.1)	0.1	0.2	0.1	0.5	0.2	0.5	0.2
λ	0.170	0.175	0.175	0.175	0.225	0.235	0.250	0.180
R^b	1.18	1.14	1.12	1.09	1.07	1.04	1.01	1.09

[a] In $cm^{-1} \times 10^{-4}$, except for λ; error limits are given in parentheses for (**2**) and apply to all other compounds. Note that: $D = b_2^0$; $3E = b_2^2$; $\lambda = E/D$. [b] Ionic radius (Å) of host cation. For M^{3+} in eight-co-ordinate compounds (Gd^{3+} 1.06 Å); for Th^{4+} nine-co-ordination. Data from S. P. Sinha, *Struct. Bonding (Berlin)*, 1976, **25**, 69.

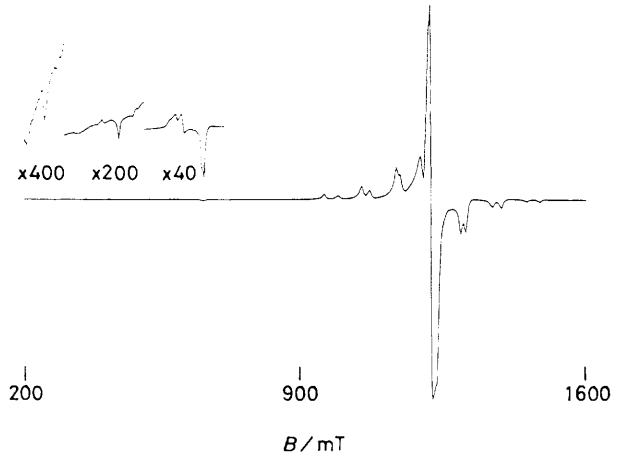

Figure 8. A typical e.s.r. spectrum at *Q*-band frequency of a gadolinium(III)-doped powder sample of compound (**7**)

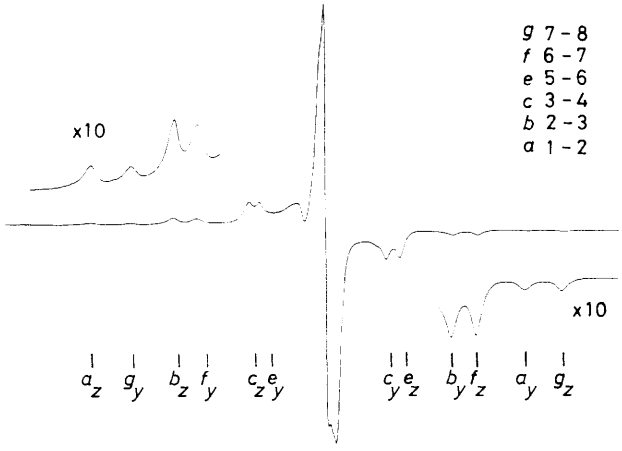

Figure 9. The spin-allowed ($\Delta M_s = \pm 1$) transitions, with their assignments, in a gadolinium(III)-doped powder sample of compound (**7**)

where μ_B is the Bohr magneton, the O_n^m are Stevens operator equivalents, and the b_n^m are corresponding spin-Hamiltonian parameters. No term is included for the interaction of the unpaired spin with the nuclear spin, *i.e.* the hyperfine interaction, as it is rarely resolved. The summation over m and n can often be greatly reduced by considering the local symmetry of the gadolinium centre. In all the compounds discussed here the actual site symmetry of the host cation is C_1. However it is still possible to treat the spectra as being due to an orthorhombic site (*i.e.* three orthogonal C_2 axes). This is done by choosing these orthogonal axes so they correspond to the principal electric field axes. Therefore the direction of the applied magnetic field H corresponding to the absolute extreme of the e.s.r. line positions was chosen as the z axis; the next most extreme position was chosen as the y axis. This allows the observed resonances to be assigned as in Figure 9. The procedure has been used before to interpret gadolinium(III) spectra in low-symmetry sites.[9]

Thus equation (1) reduces to (2). At this stage it is possible to

$$\mathcal{H} = g\mu_B\vec{H} \cdot \vec{S} + \tfrac{1}{3}(b_2^0O_2^0 + b_2^2O_2^2) + \tfrac{1}{60}(b_4^0O_4^0 + b_4^2O_4^2 + b_4^4O_4^4) + \tfrac{1}{1260}(b_6^0O_6^0 + b_6^2O_6^2 + b_6^4O_6^4 + b_6^6O_6^6) \quad (2)$$

neglect several of the higher-order terms, namely b_4^4, b_6^2, b_6^4, and b_6^6, as they are much smaller than the other terms. The magnitude of the remaining spin-Hamiltonian parameters can then be calculated using the equations given in the Appendix.[2] These parameters for compounds (**2**), (**3**), (**5**)—(**7**), (**9**), (**15**), and (**16**) are given in Table 6.

It is immediately clear that the second-order crystal-field parameters, b_2^0 and b_2^2, are much larger than those of higher order. This is generally the case for Gd^{III} in fields of axial or lower symmetry.[2,10] This consideration reduces equation (2) still further to (3), which is very similar to the spin-Hamiltonian used in interpreting $S = \frac{5}{2}$ spectra [equation (4)] where D and λ

$$\mathcal{H} = g\mu_B\vec{H} \cdot \vec{S} + \tfrac{1}{3}(b_2^0O_2^0 + b_2^2O_2^2) \quad (3)$$

$$\mathcal{H} = g\mu_B\vec{H} \cdot \vec{S} + \tfrac{1}{3}DO_2^0 + EO_2^2 \quad (4)$$

($= E/D$) are the zero-field splitting parameters,[2,11] so that $b_2^0 \equiv D$ and $b_2^2 \equiv 3E$, $\lambda = E/D \equiv b_2^2/3b_2^0$. A computer fit was carried out using the program ESRS.[3] Good agreement was found using the calculated second-order parameters, the largest single error being 6 mT in 1 500 mT, mean error 2 mT in 1 200 mT.

No conclusions can be drawn from the higher-order spin-Hamiltonian parameters as there is no statistically significant difference between them. However the second-order parameters divide the compounds into three groups. Group one contains compounds (**2**), (**3**), (**5**), and (**6**) which have the smallest D and smallest λ values. Group two contains compounds (**7**), (**9**), and (**15**) and these have larger λ values and slightly larger D values. The thorium(IV) compound, (**16**), stands alone, having by far the largest D value while having a λ value close to that of the first group. [These differences are not related to the structural differences observed in the *X*-ray analysis, as compound (**7**) is isostructural with (**2**), (**3**), (**5**), and (**6**).]

The most obvious explanation for the variation in D values is that it is related chiefly to the charge on the host cation. This would account for the general similarity within the

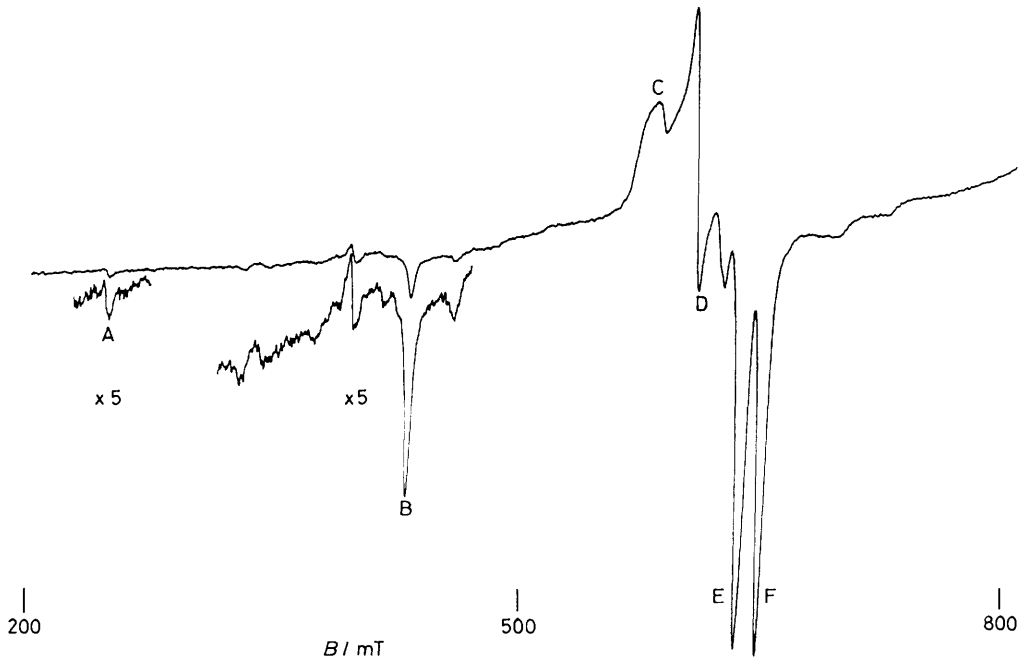

Figure 10. The low-field region of a representative gadolinium(III)-doped powder sample, (**5**), showing the high-order transitions and their assignments

Table 7. Observed spin-forbidden bands (in mT)[a] for complexes (**2**), (**5**), (**7**), (**9**), (**15**), and (**16**)

Band[b]	(2)	(5)	(7)	(9)	(15)	(16)	ΔM_s
A		248		250	253	249	±5
		330				365	±4
	394	395	397	398	398	391	±3
B	433	433	417	439	439	456	±3
	461	459		473	475		±3
C	581	581	587	581	580	566	±2
D	606	606	614	601	599	604	±2
	622	620	619	636	638		
E	637	636	634	647	650	660	±2
F	651	650	648	653	653	675	±2
	693	689		709			±2
		718		731			±2

[a] Estimated error limits of ±1 mT. [b] See Figure 10.

Table 8. Observed and calculated Q-band e.s.r. bands (in mT) for complex (**5**)

Band	Energy levels[a]	Obs.	Calc.[b]	T.p.[c]	Field direction θ, φ (°)
A	2—7	248	247	0.001	51, 90
	3—7	330	332	0.002	71, 90
	3—6[d]	395			Out-of-plane
B	3—6	433	433	0.03	42, 90
	4—7	459	460	0.006	81, 90
C	3—5, 4—6[d]	581			Out-of-plane
D	4—6	606	606	0.31	66, 0
		620			
E	4—6	636	638	0.21	65, 90
F	3—5	650	651	0.19	22, 90
	5—7[d]	689			Out-of-plane
	2—4[d]	718			Out-of-plane

[a] In order of increasing energy, 1 to 8. [b] Using g = 1.99, D = 0.038 cm^{-1}, λ = 0.175, and ν = 33.865 GHz. [c] Single-crystal transition probability. [d] Assignment made from sub-spectra (see text).

Table 9. Observed and calculated Q-band e.s.r. bands (in mT) for complex (**9**)

Band	Energy levels[a]	Obs.	Calc.[b]	T.p.[c]	Field direction θ, φ (°)
A	2—7	250	248	0.003	47, 90
	3—6[d]	398			Out-of-plane
B	3—6	439	440	0.053	43, 90
	4—7	473	473	0.011	79, 90
	2—5	488	491	0.007	9, 90
C	3—5, 4—6[d]	581			Out-of-plane
D	4—6	601	600	0.121	64, 0
		636			
E	4—6	647	647	0.344	63, 90
F	3—5	653	656	0.265	24, 90
	5—7[d]	709			Out-of-plane
	2—4[d]	731			Out-of-plane

[a] In order of increasing energy, 1 to 8. [b] Using g = 1.99, D = 0.041 cm^{-1}, λ = 0.235, and ν = 33.868 GHz. [c] Single-crystal transition probability. [d] Assignment made from sub-spectra (see text).

lanthanoid(III) compounds with the only sharp deviation occurring for Th^{IV}, *i.e.* compound (**16**).

The variation in λ values is more subtle, but generally it appears to follow the ionic radii, the smaller the ionic radii of the host cation the larger is the λ value.

It has been suggested[8] that b_2^0 and b_2^2 vary linearly with ionic radii. However previous evidence gathered from single crystal e.s.r studies seems inconclusive. For Gd^{III} in lanthanide triacetate tetrahydrates[12] b_2^2 varies linearly with ionic radii but b_2^0 does not; for Gd^{III} in lanthanide trifluorides[13] b_2^0 varies linearly with ionic radii but b_2^2 does not; for Gd^{III} in lanthanide trinitrate hexahydrates[14] neither parameter varies linearly with ionic radii in a satisfactory way for all lanthanides. Our own results tend to suggest that b_2^2 and λ may vary with ionic radii (though not linearly) but b_2^0 does not.

Low-field bands. The weak bands to low field arise from off-axis, forbidden ($\Delta M_s \neq \pm 1$) transitions. Weak bands of this

Table 10. Observed and calculated Q-band e.s.r. bands (in mT) for complex (**16**)

Band	Energy levels[a]	Obs.	Calc.[b]	T.p.[c]	Field direction θ, φ (°)
	2—8	n.s.[d]	143	0.002	28, 90
A	2—7	249	245	0.013	47, 90
	2—6	n.s.	258	0.002	90, 47
	3—7	365	350	0.011	73, 90
	3—6	391	391	0.013	90, 75
	3—6	n.s.	422	0.004	30, 0
B	3—6	456	457	0.120	41, 90
	4—7	*e*	487	0.035	76, 90
	2—5	*e*	525	0.021	11, 90
C	3—5	566	569	0.049	90, 26
D	4—6	604	605	0.333	57, 0
E	4—6	660	660	0.535	60, 90
F	3—5	675	679	0.479	26, 90

[a] In order of increasing energy, 1 to 8. [b] Using $g = 1.99$, $D = 0.055$ cm^{-1}, $\lambda = 0.18$, and $\nu = 33.854$ GHz. [c] Single-crystal transition probability. [d] n.s. = not seen. [e] Obscured by the $\Delta M_s = \pm 2$ bands.

type have been reported for some single crystals [8] but not, as far as we are aware, for powdered samples.[15]

The resonance field values of these bands for the compounds we have studied are listed in Table 7, and a representative spectrum in this region is shown in more detail in Figure 10.

The majority of these features can be shown to arise from off-axis, in-plane turning points of high-order transitions, and they can be assigned using the program ESRS [3] (Tables 8–10). The four most intense resonances (C—F), in the 570—700 mT range, are due to $\Delta M_s = \pm 2$ transitions and in the case of D—F they can be assigned as arising from in-plane turning points.

The broad peak C, however, is due to the overlap of off-axis, out-of-plane transitions between energy levels 4—6 and 3—5. This assignment could not be made in the same way as for peaks D—F, but was effected by spectral simulations using a modification [16] of ESRS, which allows sub-spectra due to individual transitions to be predicted. The weak, broad bands at *ca.* 700 mT can also be assigned in this way.

The next most intense peaks, between 300 and 500 mT, are due to $\Delta M_s = \pm 3$, or ± 4 transitions, as assigned in Tables 8—10. The weakest feature, A, at *ca.* 250 mT is due to a $\Delta M_s = \pm 5$ transition. This has a very low transition probability (*ca.* $\leqslant 0.01$) and we could not observe it in the spectra of compound (**2**) or (**7**) and it may have been obscured by background noise.

It is interesting that these higher-order bands can be seen in the spectra of powdered samples and that they can, in the main, be satisfactorily assigned using parameters obtained from the simplified spin-Hamiltonian. As the band energies appear to depend on the host metal ion in this closely related set of complexes, it would be instructive to see if such bands appear in the spectra of powdered samples of other gadolinium-doped compounds.

Appendix

Equations (A1)—(A5), taken from ref. 2, were used to calculate the spin-Hamiltonian parameters from the e.s.r. data. Here H_{az} is the transition between levels 1 and 2 in the z direction, *etc.* as given in Figure 9; b_n^m are spin-Hamiltonian parameters, φ is the angle between the magnetic field and the x-axis (here chosen as 90°). In all calculations $g = 1.99$.

$$H_{az} - H_{gz} = -(12b_2^0 + 40b_4^0 + 12b_6^0)(g\mu_B)^{-1} \quad \text{(A1)}$$

$$H_{bz} - H_{fz} = -(8b_2^0 - 20b_4^0 - 28b_6^0)(g\mu_B)^{-1} \quad \text{(A2)}$$

$$H_{cz} - H_{ez} = -(4b_2^0 - 24b_4^0 + 28b_6^0)(g\mu_B)^{-1} \quad \text{(A3)}$$

$$H_{ay} - H_{gy} = [6b_2^0 - 15b_4^0 + (15/4)b_6^0 - 6b_2^2 \cos 2\varphi - 5b_4^4 \cos 4\varphi](g\mu_B)^{-1} \quad \text{(A4)}$$

$$H_{by} - H_{fy} = [4b_2^0 + (15/2)b_4^0 - (35/4)b_6^0 - 4b_2^2 \cos 2\varphi + (5/2)b_4^4 \cos 4\varphi](g\mu_B)^{-1} \quad \text{(A5)}$$

Acknowledgements

We thank the S.E.R.C for a Research Studentship (to R. E. P. W.) and for the diffractometer and e.s.r. spectrometer. We are indebted to Dr. P. Beardwood for the use of the modified ESRS program and for helpful discussions.

References

1 D. M. L. Goodgame, D. J. Williams, and R. E. P. Winpenny, *Angew. Chem., Int. Ed. Engl.*, (*a*) 1987, **26**, 1044; (*b*) 1988, **27**, 261; (*c*) *J. Chem. Soc., Chem. Commun.*, 1988, 437; (*d*) *Polyhedron*, 1988, **7**, 1299.
2 R. W. Reynolds, L. A. Boatner, C. B. Finch, A. Chatelain, and M. M. Abraham, *J. Chem. Phys.*, 1972, **56**, 5607.
3 D. Vivien and J. F. Gibson, *J. Chem. Soc., Faraday Trans. 2*, 1975, 1640.
4 G. M. Sheldrick, SHELXTL, An Integrated System for Solving, Refining, and Displaying Crystal Structures from Diffraction Data, University of Göttingen, Federal Republic of Germany, 1978; Revision 4.1, 1983.
5 'International Tables for *X*-Ray Crystallography,' Kynoch Press, Birmingham, 1974, vol. 4, pp. 99-149.
6 D. M. L. Goodgame, D. J. Williams, and R. E. P. Winpenny, *Polyhedron*, 1988, **7**, 1807.
7 K. K. Bhandary and H. Marokar, *Acta Crystallogr., Sect. B*, 1976, **32**, 861.
8 S. K. Misra and G. C. Upreti, *Magn. Reson. Rev.*, 1986, **10**, 333.
9 M. Rappaz, M. M. Abraham, J. O. Raney, and L. A. Boatner, *Phys. Rev. B*, 1981, **23**, 1012.
10 V. B. Kravchenko, I. A. Gavrilov, A. T. Sobolev, O. F. Dudnik, and B. I. Kryuchkov, *Sov. Phys. Solid State*, 1969, **11**, 2898; G. B. Singh and P. Venkateswarlu, *Proc. Indian Acad. Sci., Sect. A*, 1967, **65**, 211.
11 R. B. Birdy and M. Goodgame, *J. Chem. Soc., Dalton Trans.*, 1982, 142.
12 S. K. Misra, M. Bartkowski, and P. Mikolajczak, *J. Chem. Phys.*, 1983, **78**, 5369.
13 S. K. Misra, P. Mikolajczak, and S. Korczak, *J. Chem. Phys.*, 1981, **74**, 922.
14 S. K. Misra and P. Mikolajczak, *J. Chem. Phys.*, 1978, **69**, 3093.
15 Y. Teki, T. Takui, and K. Itoh, *J. Chem. Phys.*, 1988, **88**, 6134.
16 P. Beardwood, unpublished work.

Received 25th August 1988; *Paper* 8/03443E